GLOBAL VIEW OF REAL-TIME TRMM MULTISATELLITE PRECIPITATION ANALYSIS

Implications for Its Successor Global Precipitation Measurement Mission

BY BIN YONG, DIE LIU, JONATHAN J. GOURLEY, YUDONG TIAN, GEORGE J. HUFFMAN, LILIANG REN, AND YANG HONG

The global error characteristics of Tropical Rainfall Measuring Mission (TRMM)-based "best effort" real-time precipitation estimates and their regional and seasonal variations are benchmarked as a baseline for its successor Global Precipitation Measurement (GPM) mission.

Precipitation is a key component of the global water cycle (Allen and Ingram 2002; Wu et al. 2013). The measurement of precipitation at global scale is therefore crucial for a comprehensive understanding of the climate, weather, hydrology, and ecological systems (Wentz et al. 2007; Bunde et al. 2013; Liu et al. 2013). However, precisely measuring precipitation in many regions of Earth is still a challenging task owing to the high spatial variability of precipitation and the sparseness of the surface-based observing networks (Ebert et al. 2007; Min et al. 2011). Especially over oceans, deserts, and mountainous areas, it is mostly infeasible to fully monitor precipitation with conventional rain gauge networks or weather radars. Satellite-based remote sensing can offer an alternative source of precipitation information for vast areas of Earth's surface and has presently become the only practical way to measure precipitation on a global basis (Tian and Peters-Lidard 2010; Kidd et al. 2012).

An important new program for global precipitation estimation is the Global Precipitation Measurement

AFFILIATIONS: YONG, LIU, AND REN—State Key Laboratory of Hydrology-Water Resources and Hydraulic Engineering, Hohai University, Nanjing, China; GOURLEY—NOAA/National Severe Storms Laboratory, Norman, Oklahoma; TIAN—Hydrological Sciences Branch, NASA Goddard Space Flight Center, Greenbelt, Maryland, and Earth System Science Interdisciplinary Center, University of Maryland, College Park, College Park, Maryland; HUFFMAN—Mesoscale Atmospheric Processes Laboratory, NASA Goddard Space Flight Center, Greenbelt, Maryland; HONG—Advanced Radar Research Center, National Weather Center, and School of Civil Engineering and Environmental Science, University of Oklahoma, Norman, Oklahoma

CORRESPONDING AUTHORS: Dr. Bin Yong, State Key Laboratory of Hydrology–Water Resources and Hydraulic Engineering, Hohai University, 1 Xikang Road, Nanjing 210098, China
E-mail: yongbin_hhu@126.com; yanghong@ou.edu

The abstract for this article can be found in this issue, following the table of contents.

DOI:10.1175/BAMS-D-14-00017.1

In final form 14 June 2014
©2015 American Meteorological Society

(GPM) mission lead by the National Aeronautics and Space Administration (NASA) and the Japan Aerospace Exploration Agency (JAXA) (Kidd and Huffman 2011). The GPM is composed of one Core Observatory satellite and approximately eight constellation satellites. The GPM Core Observatory was successfully launched by the H-IIA launch vehicle 23 at 1307 EST 28 February 2014 (www.jaxa.jp/countdown/f23). This core satellite carries a dual-frequency precipitation radar (DPR; the Ku-band at 13.6 GHz and Ka-band at 35.5 GHz) and a multichannel GPM microwave imager (GMI; frequency range between 10 and 183 GHz), which will be used together to develop a new calibration standard for the other microwave radiometers on the constellation satellites (Tapiador et al. 2012; Hou et al. 2014). In addition to these passive microwave sensors aboard low-Earth-orbiting (LEO) satellite, GPM will utilize infrared measurements from geostationary satellites, yielding precipitation estimates around the globe at 0.1°, 30-min resolution. In general, the Core Observatory will help to observe worldwide precipitation (rain and snowfall) rates several times per day. Therefore, it is anticipated that GPM will improve climate, weather, and hydrological predictions through more accurate and more frequent precipitation measurements from space, aiming for a 3-h interval for the LEO microwave observations. This should help meteorologists to better understand how Earth's hydrological cycle works.

As a prelude to GPM, the current operational Tropical Rainfall Measuring Mission (TRMM) Multisatellite Precipitation Analysis (TMPA) system produces estimates of quasi-global rainfall (50°N–50°S) at relatively fine resolution (0.25° × 0.25°, 3 h) (Huffman et al. 2007; Yong et al. 2013). The TMPA is computed twice—first in near-real time (TMPA-RT; 6–9 h after observation time), and then again in post-real time (TMPA-P; two months latency) for research purposes. These two types of TMPA standard products have been widely utilized in a variety of research and operational applications (Villarini and Krajewski 2007; Habib et al. 2009; Kidd et al. 2009; Tobin and Bennett 2010; Behrangi et al. 2011; Khan et al. 2011; Romilly and Gebremichael 2011; Habib et al. 2012; Wu et al. 2012; among many others). Prior studies indicate that the TMPA-RT estimates are less accurate than TMPA-P due to the lack of month-to-month gauge adjustments and high-quality TRMM combined instrument (TCI) calibration in the data processing algorithm (Su et al. 2008; Stisen and Sandholt 2010; Yong et al. 2010; Bitew and Gebremichael 2011). However, it is the near-real-time availability that makes TMPA-RT attractive for real-time hydrological forecasting and natural hazard warning at local, regional, and even global scales (e.g., Hossain and Lettenmaier 2006; Hong et al. 2007; Gourley et al. 2013).

During the past decade, the TMPA real-time system has undergone three major upgrades (corresponding to versions 5, 6, and 7) because of the new sensors and upgraded algorithms [see Yong et al. (2010, 2012) for a detailed description]. As one of the most important algorithmic upgrades, a climatological calibration algorithm (CCA) was applied in TMPA's real-time estimates from 1 October 2008 in version 6, utilizing climatological gauge information to effectively reduce systematic biases, while maintaining the near-real-time availability. For this monthly calibration procedure, the developers first determined a local histogram matching of the TRMM Microwave Imager (TMI) to TCI, computed from 14 years of coincident data (in version 7) to establish the climatology for each calendar month. Then, a monthly climatological calibration of TCI to 3B43 (another TRMM product computed at monthly time intervals) is calculated as a simple ratio on a 1° × 1° grid. The calibration factor is aggregated to an overlapping 3° × 3° boxcar template using 14 years of data. Finally, the TMI-TCI and TCI-3B43 calibrations are applied sequentially to the preliminary real-time products to create the calibrated TMPA-RT estimates.

The CCA is the primary upgrade from version 5 to version 6. Furthermore, this new calibration has been used in the current version 7, and a similar approach will carry over to the real-time runs of the Integrated Multisatellite Retrievals for GPM (IMERG) algorithm. Version 7 also introduced some newer passive microwave (PMW) and infrared (IR) sensors relative to version 6, mainly including the Special Sensor Microwave Imager/Sounder (SSMIS) F16 and F17, Microwave Humidity Sounder (MHS) (N18 and N19), Meteorological Operational satellite program (MetOp), and the 0.07° Gridsat-B1 infrared data (http://trmm.gsfc.nasa.gov/).

As the GPM era is now upon us, studies will focus on the impact of the contemporary measurements as well as continued algorithm development. Therefore, it seems timely for this paper to provide some insights into the following questions frequently posed by the satellite quantitative precipitation estimation (QPE)-hydrology community: 1) How do the latest version 7 TMPA-RT estimates perform at global scale (specifically compared to version 6)? 2) Are the current TMPA precipitation algorithm concepts being used in the new IMERG system ready for GPM?

Because of the lack of accurate and independent ground observations, we cannot directly quantify the systematic errors of TMPA-RT estimates by surface validation data across the entire globe. To provide a globally consistent evaluation, we first use the version 7 TMPA-P product as the reference for our comparisons in this study for the following reasons. First, it ingests the new Global Precipitation Climatology Centre (GPCC; Rudolf et al. 1994) "full" gauge analysis, and hence essentially reproduces the precipitation characteristics of the gridded GPCC dataset at monthly scale in many land areas. Through these gauge adjustments, which also introduce rainfall patterns forced by orography, the research product has been shown to successfully remove systematic biases of satellite retrievals (Chen et al. 2013a,b). Moreover, the TMPA developers attempted to make the real-time datasets resemble TMPA-P as much as possible through the CCA calibration to TCI. Therefore, the latest version 7 TMPA-P research product gives us a suitable reference to compare different TMPA real-time estimates on a global basis. The drawback is its lack of independence from the real-time products being evaluated; the research product incorporated the same remote sensing measurements in the final products. In this paper, the "previous" uncalibrated and the "new" climatologically calibrated TMPA-RT estimates for both version 6 (RTV6_UC and RTV6_C, respectively) and version 7 (RTV7_UC and RTV7_C, respectively) are statistically investigated against version 7 TMPA-P (V7 hereafter) at the global scale. We also employed a gauge-based analysis of daily precipitation produced by the National Oceanic and Atmospheric Administration's (NOAA's) Climate Prediction Center (CPC; ftp://ftp.cpc.ncep.noaa.gov/precip/CPC_UNI_PRCP/) (Chen et al. 2008; Xie et al. 2010) to further evaluate the TMPA-RT precipitation products over four densely gauged regions. We selected an overlapping timespan of these six available datasets, three complete years from July 2008 to June 2011.

RESULTS AND DISCUSSION. *Global view of systematic biases in TMPA-RT estimates.* A global map of mean daily precipitation difference between the four TMPA real-time estimates (RTV6_UC, RTV6_C, RTV7_UC, and RTV7_C) and the V7 post-real-time research product gives a clear indication of where the datasets are performing better or worse. In general, RTV6_C and RTV7_C have lower relative biases than their corresponding uncalibrated estimates (Fig. 1). Most notably along the western Pacific Ocean convergence zone (near 10°S) extending over the Philippines, Indonesia, and Malaysian Islands, southeastern China, and into the Indian Ocean, the CCA calibration significantly elevated the uncalibrated TMPA-RT estimates so as to effectively reduce their substantial negative biases. Similar patterns were also found in the narrow intertropical convergence zone across the Atlantic Ocean extending toward Central America. Likewise, such upward adjustments also alleviate the systematic underestimation along most coastlines (e.g., the western coast of India and the eastern coast of North America) and over inland water bodies (e.g., the Great Lakes).

From Fig. 2, it can be seen that these extreme negative biases primarily occurred in the boreal warm season [June–August (JJA)]. The patterns of underestimation by the uncalibrated products seem to correspond to climatological maxima of tropical rain features and the migration of the Asian summer monsoon. On the other hand, there is an apparent overestimation with the RTV6_UC and RTV7_UC datasets in central Africa (an area just to the west of Lake Victoria; see Figs. 1a and 1c), especially during the rainy seasons (refer to plots of "MAM" and "SON" in Fig. 2). Over this region, significant reductions resulted following the CCA calibration, thereby reducing the most significant positive biases for the uncalibrated TMPA-RT products.

Over land, almost all regions exhibit strong seasonality of bias. For example, Europe has much larger negative biases in winter due to erroneous retrievals of snow events during the cold season (Yong et al. 2013). Over the eastern continental United States (CONUS), the negative biases with the RTV6_UC and RTV7_UC estimates were also likely the result of snow events. A positive bias appears in the Great Plains of the United States presumably due to overestimation by the PMW-based land algorithms for strong convective events during the warm season (Tian et al. 2009; Gourley et al. 2010). Intercomparing the TMPA-RT estimates before and after climatological calibration, one can see that the CCA substantially improved these seasonal errors and biases for both versions (Fig. 2).

Many of the global error features in TMPA-RT estimates can be related to the overpass frequency and retrieval characteristics of the PMW and IR sensors incorporated. Two types of PMW sensors are currently available for TMPA: conical-scanning imagers, including TMI, the Advanced Microwave Scanning Radiometer (AMSR), the Special Sensor Microwave Imager (SSM/I), and SSMIS; and cross-track-scanning sounders including Advanced Microwave Sounding Unit (AMSU) and Microwave Humidity Sounder (MHS). Generally, the imagers have better

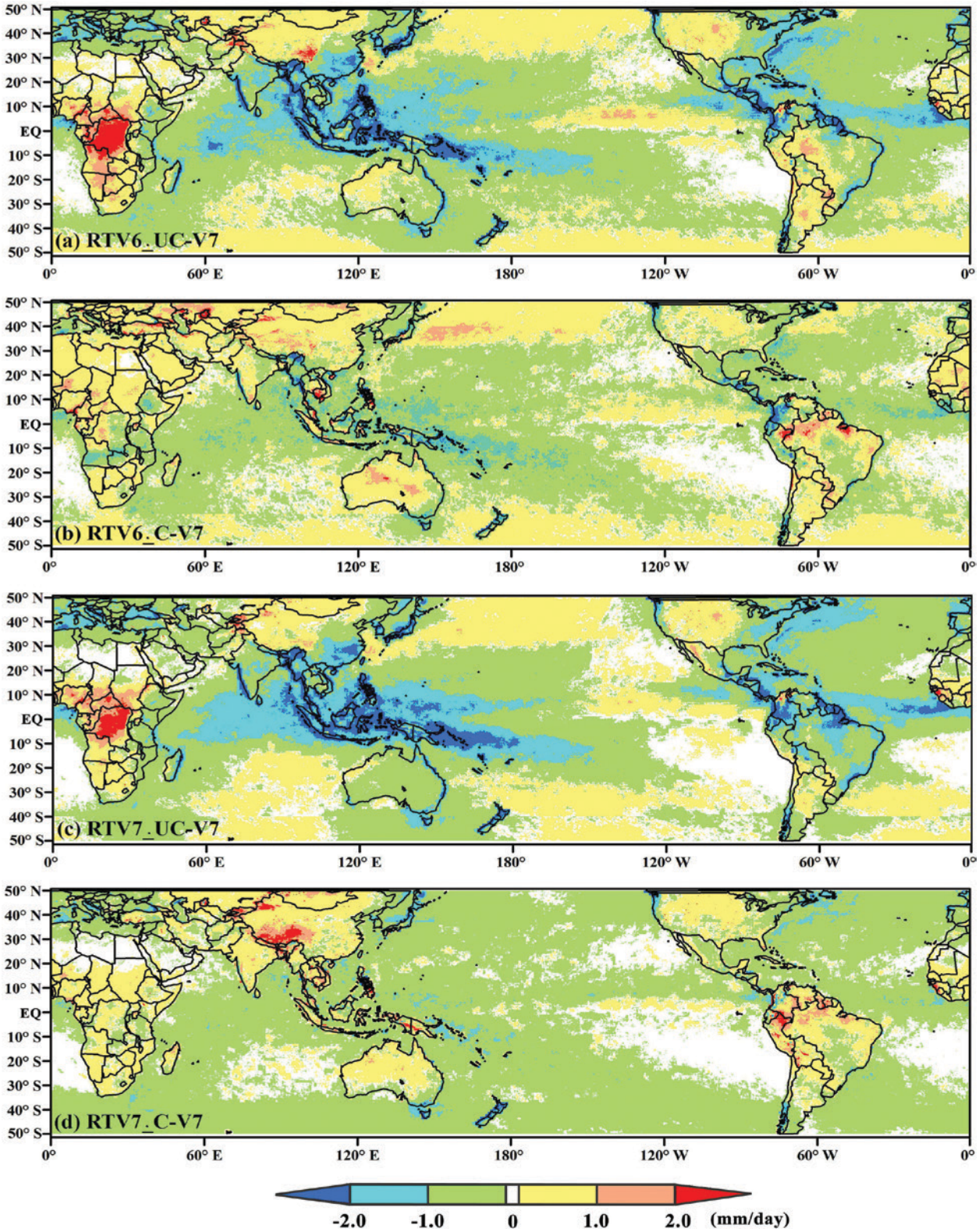

Fig. 1. Global map of mean daily precipitation difference between (a) RTV6_UC and production V7, (b) RTV6_C and production V7, (c) RTV7_UC and production V7, and (d) RTV7_C and production V7 for the 3-yr study period (Jul 2008–Jun 2011).

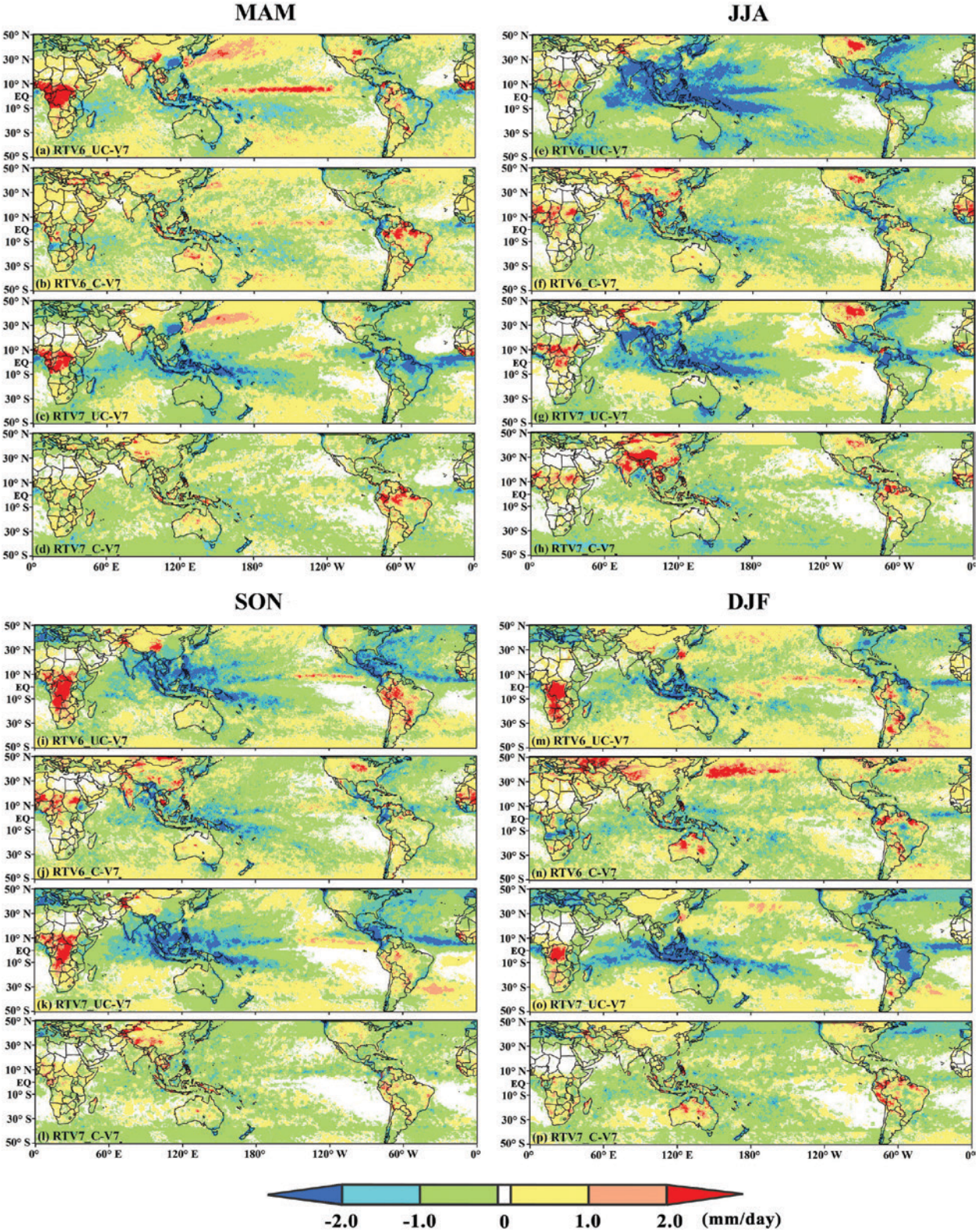

Fig. 2. As in Fig. 1, but for seasonal variations: boreal (a)–(d) spring (Mar–May), (e)–(h) summer (Jun–Aug), (i)–(l) autumn (Sep–Nov), and (m)–(p) winter (Dec–Feb).

performance than the sounders (Lin and Hou 2008; Tang et al. 2014), and TMPA version 7 system is using more imager overpasses than version 6 on the global scale (see Figs. 3e,f). [Note that the TMPA selects imager data over sounders when both are available in a grid box at a particular 3-h time.] This is an improvement that takes advantage of more and better data sources for producing merged version 7 TMPA estimates. In addition, the proportion of geostationary infrared-based retrievals (geo-IR) is reduced when compared to version 6 (Figs. 3g,h). However, the Tibetan Plateau is an exception. Over this region, the usage of geo-IR data with poor correlation to precipitation is more frequent than the previous version (its scanning proportion accounting for over 70% of total scans), likely due to more stringent quality control of the PMW overpasses as they are unreliable over the snow cover and complex terrain in the Tibetan Plateau. Therefore, the geo-IR data are less certain given that they are calibrated by the deficient PMW over this region. On the other hand, geo-IR data themselves are not necessary more reliable, because of many orographic rain events lacking the strong convective signatures for geo-IR detection. Therefore, the choice of geo-IR or PMW data sources over this area is equally challenging, and the fact that version

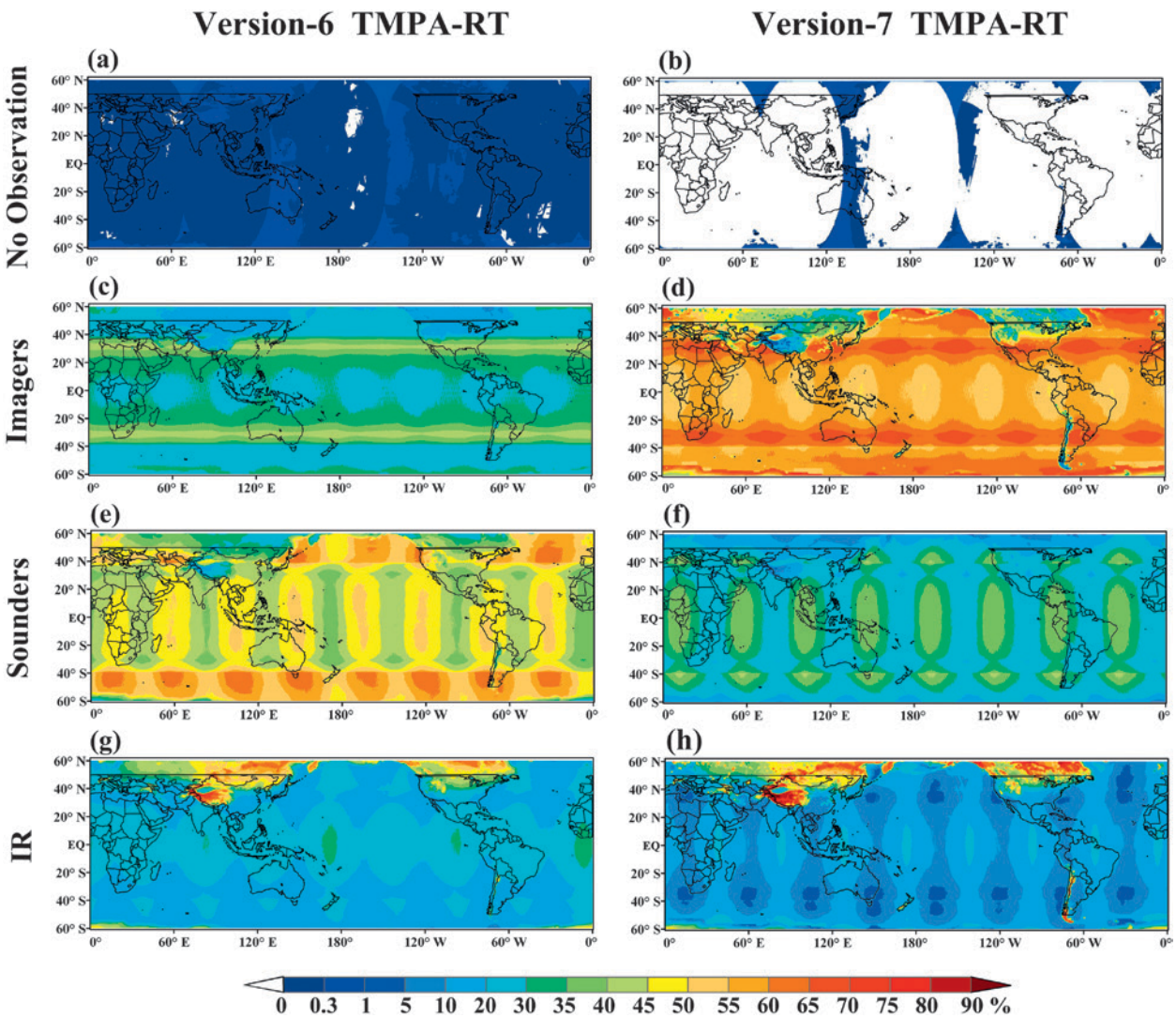

Fig. 3. Global distribution of scan frequency of various microwave sensors introduced into the (left) version 6 and (right) version 7 TMPA real-time system: (a),(b) no observation, (c),(d) imagers, (e),(f) sounders, and (g),(h) IR. Note: In the text, the scan frequency of a certain kind of sensor (SF_i) is defined as follows:

$$SF_i = \frac{SC_i}{SC_{total}} \times 100\%, \qquad (1)$$

where SC_i is the scan counts of a certain kind of sensor and SC_{total} is the total scan counts for all sensors.

7 utilizes more geo-IR data than version 6 is just a reflection of the large uncertainties in our knowledge for this area (Tian and Peters-Lidard 2010).

It is worth noting that the issues were not readily resolvable by calibrating to rain gauges. Relative to RTV7_UC, RTV7_C has a dramatic overestimation in the Tibetan Plateau (Fig. 1d). Such a significant discrepancy before and after climatological calibration should be attributed to the CCA algorithm. Because of high elevation, complex terrain, severe weather, and general inaccessibility, direct meteorological observations employed in the improved GPCC rain gauge analyses do not exist over large portions of the Tibetan Plateau, especially in the midwestern part of the plateau. Hence, the GPCC values used in the CCA calibration over the Tibetan Plateau were mainly determined by the gridded interpolation results of its surrounding areas (e.g., India, Southeast Asia, and southeastern China). Over these surrounding regions extending to the western Pacific Ocean and Indian Ocean, the upward adjustments of the CCA calibration evidently elevated the RTV7_UC estimates at the large scale, but meanwhile unfavorably increased the original positive biases over the Tibetan Plateau, particularly during the warm season (Figs. 2g,h). The tendency to raise precipitation amounts seems to be more significant in version 7 than in version 6 (Figs. 2e–h), which could explain the larger positive biases in RTV7_C relative to RTV6_C (Figs. 1b,d). This is an indication of the large uncertainties in the gauge data as well. A similar phenomenon can also be found in the Tian Shan north of the Himalayas and the Cordilleras in the western coastal mountains of South America. From this global analysis, we have shown that the current version 7 TMPA-RT data still have much uncertainty in high mountainous areas, especially at the Earth's "third pole."

Improvement for both land and ocean. The density-colored scatterplots displayed in Fig. 4 give additional analyses of how the CCA calibration works for two different TMPA versions over the whole domain, broken into land and ocean areas. In general, we can see that the scatterplots of calibrated TMPA-RT (bottom) have higher Pearson linear correlation coefficient (CC) and lower root-mean-square error (RMSE) and the points are clustered more closely to the 1:1 line than for the uncalibrated estimates (top). The uncalibrated TMPA-RT products substantially underestimate precipitation over both land and ocean, while the CCA calibration

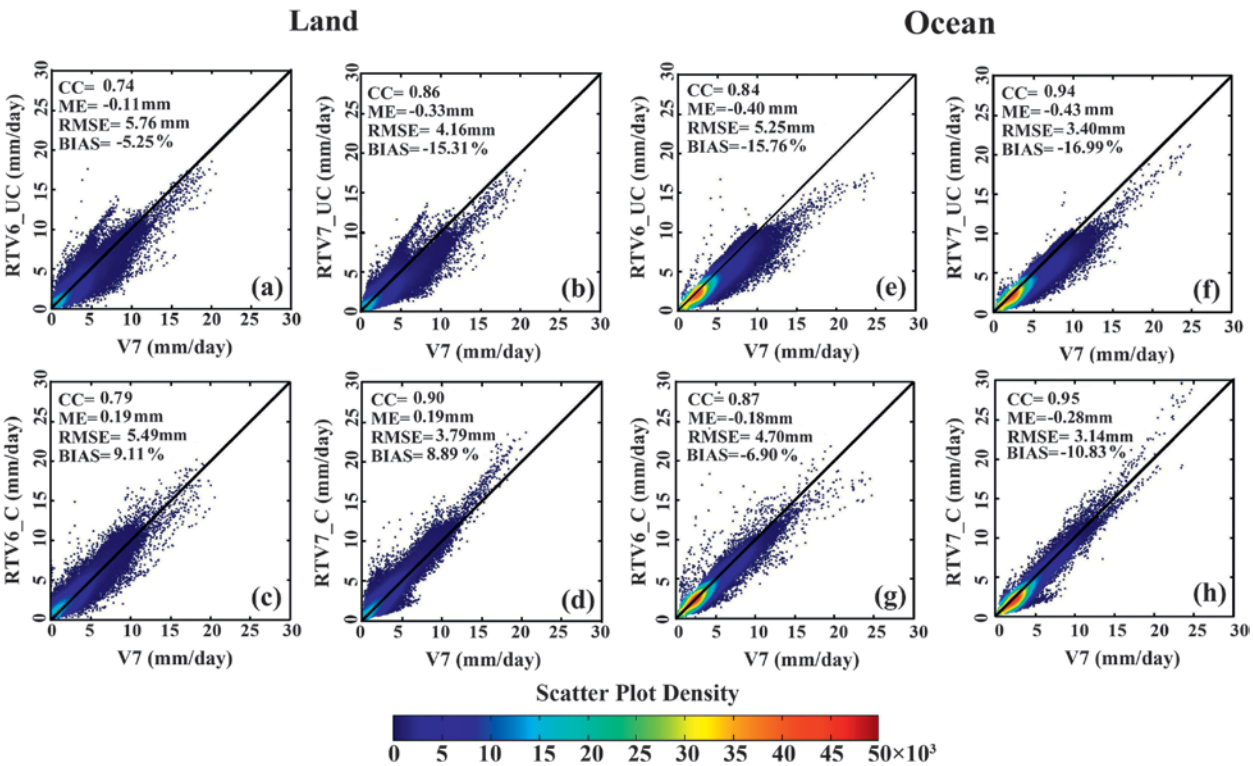

Fig. 4. Two-dimensional scatterplots of daily precipitation for (top) uncalibrated and (bottom) calibrated TMPA-RT against production V7 for (left) land and (right) ocean, corresponding to the maps in Fig. 1. Note: The formulas and meaning of all statistical indices in each plot are described in more detail in Table 1 of Yong et al. (2010).

effectively reduced such systematic negative biases. Over land, all the statistical indices indicate that the RTV7_C outperformed RTV6_C with higher correlation and lower error and bias. Over oceanic regions, the mean error (ME) and relative bias (BIAS) of RTV7_C are slightly larger than those of RTV6_C. But it cannot be considered that the latter is superior to the former, since the overall bias is the average results offset by opposing signs in different regions. The CC and RMSE are informative here, and indeed show better performance by RTV7_C. Overall, our evaluation indicates that the RTV7_C provides the best daily precipitation estimates and its systematic bias is 8.89% for land and –10.83% for ocean (benchmarked by V7). RTV7_C has better CC and lower RMSE over oceanic regions than over land. This is likely due to superior performance of the PMW algorithms over ocean.

Latitudinal profile of TMPA estimates. Figure 5 depicts the latitudinal distribution of the annual mean precipitation of the four TMPA-RT estimates against V7 over both land and ocean. From this latitudinal profile, one tends to see relatively larger and more complicated oscillations over land areas than ocean, particularly in the Northern Hemisphere. This is mainly due to the small-scale variability of continental precipitation associated with orography. Over land, the profile curves of calibrated TMPA-RT estimates are rather close to that of V7 in the deep tropics, roughly between 25°N and 18°S (Fig. 5a). The overestimation of RTV6_C and RTV7_C (corresponding to Figs. 4c and 4d, respectively) mostly appears from 25° to 50°N in the Northern Hemisphere. Furthermore, RTV7_C has significant overestimation at midlatitudes between 25° and 35°N, even worse than RTV6_C. This is because of the aforementioned retrieval and calibration issues arising from the updated version 7 system primarily over the Tibetan Plateau.

At latitudes beyond 35°N, the RTV6_C seemed to excessively elevate the uncalibrated TMPA-RT estimates (e.g., Europe, Middle East, and eastern United States; refer to Figs. 1a,b), while a relatively better performance was found for RTV7_C. Additionally, we note that the most significant underestimation with RTV6_UC and RTV7_UC occurred from 15° to 30°N. At this latitude band, the CCA calibration works best and effectively mitigates the systematic negative biases particularly in southeastern China, Southeast Asia, and India (see Fig. 1). This is mainly because of the dense ground observing networks distributed over these regions enabling robust gauge adjustments using the GPCC full analysis in the CCA calibration scheme. Relative to land,

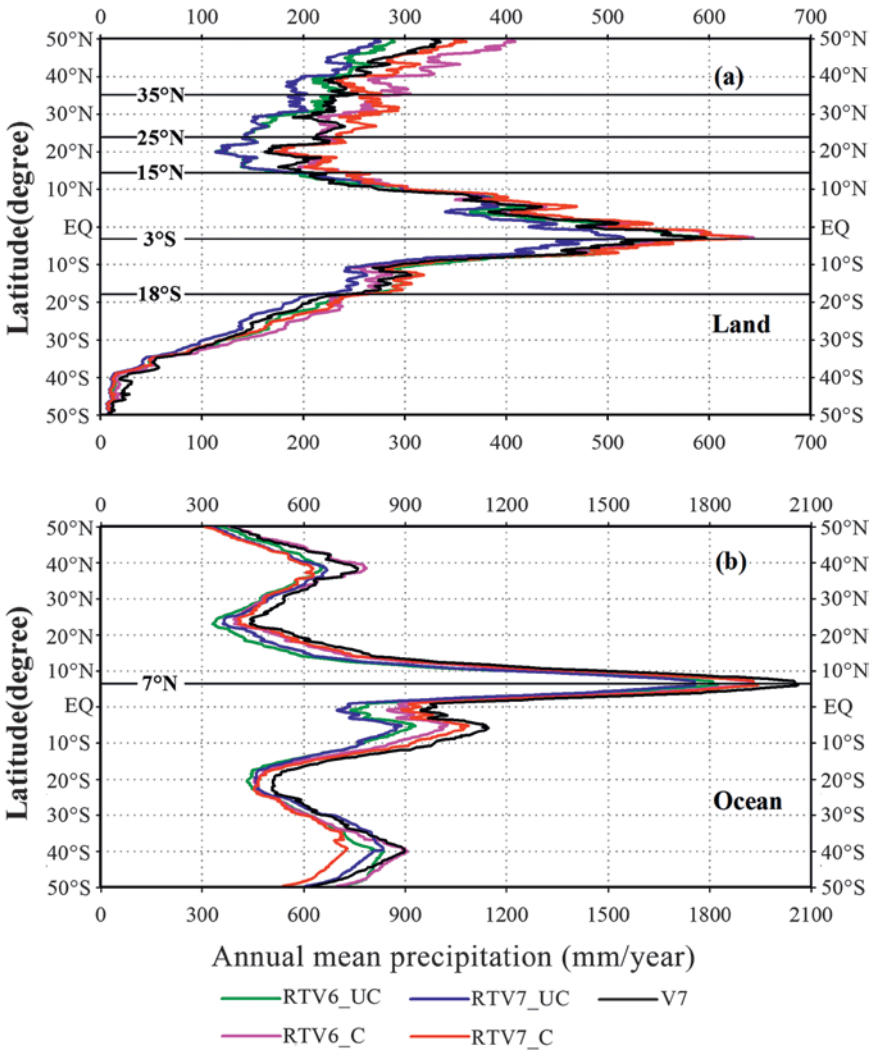

Fig. 5. Latitudinal distribution of the annual mean precipitation of four TMPA-RT estimates (RTV6_UC, RTV6_C, RTV7_UC, RTV7_C) and production V7 over both (a) land and (b) ocean.

the latitudinal profile curves over the oceans look more stable and smoother (Fig. 5b). Maximum over-ocean rainfall is situated at 7°N, while the land maximum is at about 3°S. Similar to the patterns in Fig. 5a, the systematic underestimations with uncalibrated TMPA-RT were also alleviated after the CCA calibration over the ocean, especially for the latitude band 20°N/S (Fig. 5b). But, in general, the calibrated TMPA-RT estimates still contain negative biases as compared to V7.

Evaluation of TMPA-RT estimates over the globe. The daily statistics of the four TMPA-RT datasets against the gauge-adjusted V7 product are summarized in Table 1 for land, ocean, and global domains in the latitude band 50°N/S for different seasons. First, all statistical indices with the version 6 TMPA-RT are substantially improved in most cases. However, the boreal winter season is different, with slightly lower CC and higher RMSE values found for all areas. In terms of ME and BIAS, precipitation over land seems to be elevated a little more for both the autumn and winter seasons. For version 6, most of the changes in the four representative statistical indices point to the success in the CCA calibration scheme. As for version 7, the RTV7_C estimates apparently outperformed RTV7_UC according to almost all statistics, except for slightly larger ME and BIAS values over land in summer. This arises because of the retrieval issues and lack of effective CCA calibration due to sparse rain gauges over the Himalayan region. Overall, the near-unanimous improvement after the CCA calibration over both land and ocean further confirms our spatial analysis results as presented in the prior sections. The systematic errors and biases in the original uncalibrated TMPA-RT were generally alleviated after the CCA was applied.

Table 1. Seasonal statistics of comparing daily accumulations of uncalibrated and calibrated TMPA-RT estimates (i.e., RTV6_UC, RTV7_UC, RTV6_C, and RTV7_C), taking daily V7 as the reference. Results are displayed for land, ocean, and global domains in the latitude band 50°N–50°S during the study period Jul 2008–Jun 2011. Shading indicates better statistics in each UC/C pair.

Season	Item	CC				ME (mm day^{-1})				RMSE (mm day^{-1})				BIAS (%)			
		RTV6_UC	RTV6_C	RTV7_UC	RTV7_C	RTV6_UC	RTV6_C	RTV7_UC	RTV7_C	RTV6_UC	RTV6_C	RTV7_UC	RTV7_C	RTV6_UC	RTV6_C	RTV7_UC	RTV7_C
MAM	Land	0.78	0.78	0.86	0.90	0.22	0.17	−0.31	0.14	5.54	5.42	4.06	3.69	9.36	7.33	−13.18	5.97
	Ocean	0.86	0.87	0.94	0.95	−0.08	−0.07	−0.39	−0.24	4.71	4.66	3.30	3.04	−3.25	−2.69	−15.07	−9.29
	Global	0.85	0.85	0.92	0.93	−0.004	−0.007	−0.37	−0.14	4.87	4.79	3.47	3.18	−0.18	−0.28	−15.60	−5.97
JJA	Land	0.66	0.77	0.84	0.89	−0.57	0.16	−0.29	0.37	6.76	5.95	4.57	4.27	−21.67	6.30	−11.37	14.70
	Ocean	0.78	0.87	0.94	0.95	−0.86	−0.28	−0.49	−0.32	6.29	4.78	3.46	3.20	−31.49	−10.27	−17.95	−11.98
	Global	0.76	0.85	0.92	0.93	−0.78	−0.17	−0.43	−0.14	6.30	5.04	3.74	3.48	−30.71	−6.57	−17.31	−5.75
SON	Land	0.72	0.78	0.85	0.89	−0.02	0.16	−0.20	0.11	5.95	5.33	4.19	3.63	−1.04	6.92	−8.85	4.99
	Ocean	0.83	0.88	0.95	0.95	−0.47	−0.21	−0.46	−0.25	5.47	4.64	3.42	3.08	−17.48	−7.80	−17.06	−9.18
	Global	0.81	0.86	0.92	0.94	−0.36	−0.12	−0.39	−0.15	5.51	4.76	3.60	3.20	−14.68	−4.81	−16.10	−6.34
DJF	Land	0.78	0.77	0.86	0.89	−0.05	0.30	−0.52	0.13	5.47	5.92	4.27	3.92	−2.05	12.22	−21.40	5.45
	Ocean	0.88	0.87	0.94	0.95	−0.19	−0.16	−0.40	−0.31	4.79	4.87	3.49	3.29	−7.03	−5.88	−14.87	−11.29
	Global	0.86	0.85	0.92	0.93	−0.15	−0.04	−0.43	−0.19	4.91	5.10	3.67	3.43	−6.18	−1.69	−17.39	−7.69
All Seasons	Land	0.74	0.79	0.86	0.90	−0.11	0.19	−0.33	0.19	5.76	5.49	4.16	3.79	−5.01	9.13	−15.30	8.86
	Ocean	0.84	0.87	0.94	0.95	−0.40	−0.18	−0.43	−0.28	5.25	4.70	3.40	3.14	−15.60	−6.88	−16.96	−10.81
	Global	0.81	0.85	0.92	0.93	−0.25	−0.12	−0.42	−0.18	5.28	4.92	3.61	3.30	−13.48	−3.42	−16.92	−6.62

Gauge-based validation of TMPA-RT estimates over four representative regions. Up to now, the TMPA-RT estimates were evaluated over the globe using the V7 post-real-time research product as reference. The primary advantage was the availability of matched data at each grid point over land and ocean. However, despite the research product being heavily influenced by the GPCC gauges, it uses the same remote sensing data in its estimation scheme as the TMPA-RT. Further, the CCA bias adjustment to the RT products is based on the monthly GPCC gauge accumulations. So, the evaluation was not performed with independent datasets. In this section, we adopted the CPC unified gauge-based analysis (Chen et al. 2008; Xie et al. 2010) as the reference to further evaluate the global precipitation products over land. The CPC precipitation dataset (at a daily, 0.5° × 0.5° latitude/longitude resolution) is computed by interpolating gauge observations from over 30,000 stations through the optimal interpolation (OI) algorithm of Xie et al. (2007). The degree to which the CPC dataset is different from what Huffman et al. (2010) used for the gauge analysis in TMPA-P estimates and CCA calibration is not known. However, the CPC-based analysis was performed at daily scale, which provides independent information about the random errors with the TMPA-RT products. Our quantitative validation was performed over the United States, East Asia, Europe, and Australia (see Fig. 6). The four regions were chosen because their relatively dense gauge networks can offer reliable ground verification for the TMPA-RT estimates. Furthermore, these regions cover a wide range of climate regimes and land surface characteristics (Ebert et al. 2007).

In this study, the four TMPA-RT datasets were resampled to 0.5° × 0.5° resolution corresponding to the spatial scale of the CPC gauge analysis. To reduce the uncertainty in the validation results, we only selected grid boxes that contained at least one gauge to compute the daily statistics between the TMPA-RT estimates and the CPC gauge analysis.

Table 2 summarizes the seasonal statistics before and after the CCA calibration for the four densely gauged regions. With respect to the indices of CC, ME, and BIAS, the CCA exhibits an effective improvement over its respective uncalibrated versions for all the validation regions. Taking version 7 as an example, the CCA increased the correlation between TMPA-RT and the CPC gauge observations (except in Australia during winter) and significantly reduced the ME and BIAS values. These results are consistent with our global evaluation results in the previous subsection. However, we note that the daily RMSE became worse after the calibration in most cases, such as in

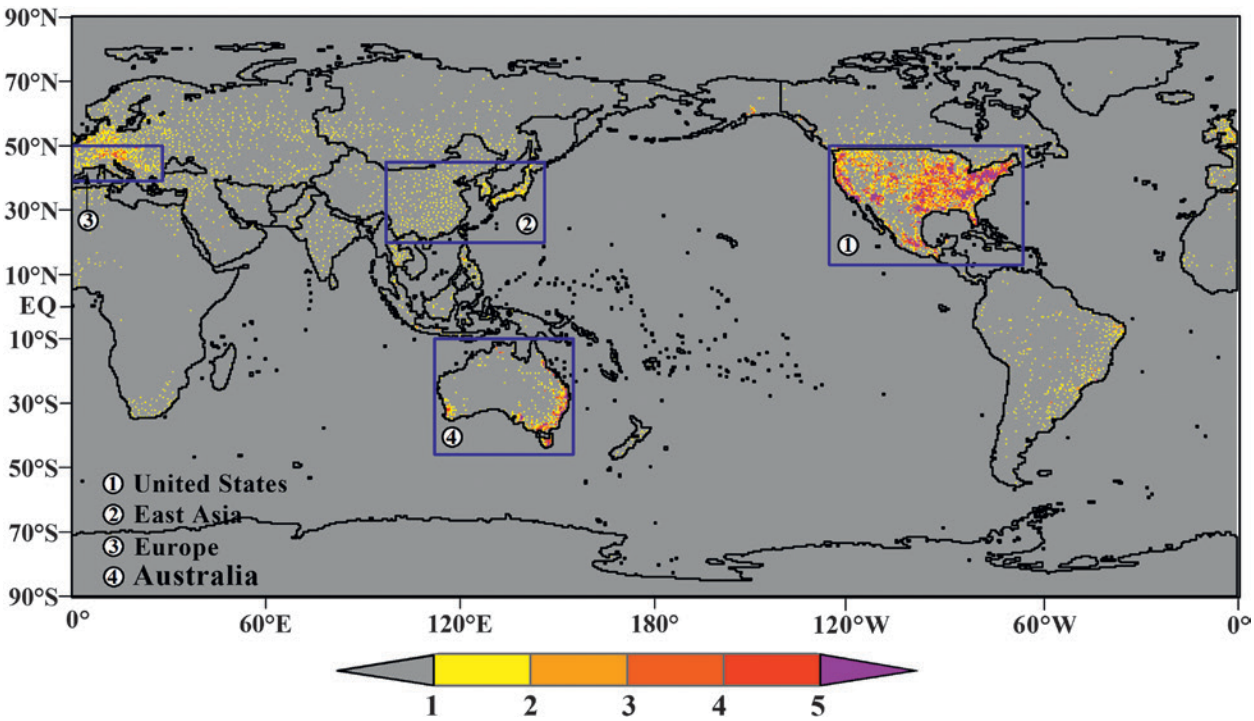

Fig. 6. Number of gauge stations in a 0.5° × 0.5° latitude/longitude grid for the CPC unified gauge-based analysis over the global land areas (July 2008–June 2011). The four selected validation regions (i.e., United States, East Asia, Europe, and Australia) are also shown.

East Asia and Australia, contrary to the results in Table 1. This implies that the CCA made the real-time estimates statistically closer to the research product, but not to the CPC gauge observations. This is likely due to the sparser gauge data used in CCA in these regions and the scale differences over which the CCA was applied relative to the daily accumulations. Since the monthly climatological calibrators in the CCA seemed to amplify the dynamic range of daily precipitation, the daily RMSE still increased despite the decreased systematic bias. The basin-scale assessment of Yong et al. (2013) shows that the CCA tends to improve on the error and bias by primarily altering the precipitation estimates at higher rain rates. The primary concern from these results is that the employment of the historical gauge data and the smooth-fill scheme in the CCA monthly bias correction could homogenize the highly variable local rainstorm characteristics. This characteristic might be unfavorable to heavy rainfall-related flood forecasting and landslide warning. Therefore, it is important to continue providing the uncalibrated real-time precipitation as an additional field in the

Table 2. Seasonal statistics of comparing daily accumulations of uncalibrated and calibrated TMPA-RT estimates (i.e., RTV6_UC, RTV7_UC, RTV6_C, and RTV7_C), taking daily CPC estimates as the reference. Results are displayed for four densely gauged regions (i.e., United States, East Asia, Europe, and Australia) during the study period Jul 2008–Jun 2011. Shading indicates better statistics in each UC/C pair.

Season	Item	CC				ME (mm day^{-1})				RMSE (mm day^{-1})				BIAS (%)			
		RTV6_UC	RTV6_C	RTV7_UC	RTV7_C	RTV6_UC	RTV6_C	RTV7_UC	RTV7_C	RTV6_UC	RTV6_C	RTV7_UC	RTV7_C	RTV6_UC	RTV6_C	RTV7_UC	RTV7_C
MAM	U.S.	0.34	0.34	0.35	0.37	−0.01	−0.48	−0.35	−0.31	8.30	7.53	7.44	7.09	−0.60	−20.07	−14.54	−12.94
	East Asia	0.45	0.46	0.47	0.51	−0.91	−0.37	−1.33	−0.57	7.05	8.25	6.78	7.30	−30.81	−12.70	−45.09	−19.47
	Europe	0.36	0.39	0.35	0.38	−0.21	0.59	−0.38	0.19	4.63	5.65	4.46	5.01	−11.53	33.41	−21.63	10.46
	Australia	0.58	0.57	0.60	0.62	−1.11	−0.43	−1.41	−0.50	7.07	7.84	6.87	7.20	−40.68	−15.78	−51.66	−18.24
JJA	U.S.	0.32	0.39	0.38	0.42	0.25	0.21	0.68	0.45	10.24	8.54	9.50	8.25	8.57	7.12	22.79	15.24
	East Asia	0.47	0.51	0.54	0.56	−1.95	0.17	−1.56	0.31	11.56	13.62	10.62	12.16	−35.43	3.16	−28.29	5.70
	Europe	0.42	0.51	0.49	0.51	−0.28	0.57	0.16	−0.11	6.14	6.16	6.23	5.35	−11.00	22.84	6.46	−4.58
	Australia	0.46	0.51	0.55	0.53	−1.32	−0.58	−1.29	−0.68	4.64	5.08	4.39	4.68	−72.68	−31.75	−70.90	−37.36
SON	U.S.	0.34	0.39	0.39	0.41	−0.67	−0.33	−0.69	−0.09	7.26	7.69	6.82	7.76	−27.73	−13.54	−28.40	−3.82
	East Asia	0.40	0.45	0.48	0.51	−1.04	−0.12	−1.08	−0.21	7.76	9.22	7.17	8.12	−39.07	−4.67	−40.86	−7.75
	Europe	0.50	0.54	0.52	0.56	−0.87	0.56	−0.91	0.03	4.90	6.38	4.84	5.55	−36.34	23.39	−37.85	1.02
	Australia	0.57	0.58	0.59	0.61	−0.68	−0.44	−0.92	−0.57	5.77	6.02	5.51	5.55	−28.85	−18.50	−38.71	−24.05
DJF	U.S.	0.30	0.30	0.31	0.31	−0.66	0.01	−0.87	−0.03	5.42	7.59	5.11	6.88	−35.50	0.50	−46.54	−1.66
	East Asia	0.24	0.27	0.28	0.33	−0.70	−0.13	−0.87	−0.41	4.31	5.90	4.08	4.85	−50.13	−9.14	−61.63	−29.24
	Europe	0.33	0.34	0.32	0.34	−1.13	0.39	−1.36	−0.69	4.62	6.95	4.55	5.19	−51.75	17.98	−62.01	−31.59
	Australia	0.63	0.64	0.62	0.65	−0.67	−0.40	−1.35	−0.29	10.67	10.92	10.36	10.60	−13.09	−7.76	−25.49	−5.65
All Seasons	U.S.	0.32	0.36	0.36	0.39	−0.27	−0.15	−0.30	0.01	7.85	8.00	7.39	7.51	−11.26	−6.07	−12.57	0.27
	East Asia	0.45	0.49	0.52	0.54	−1.15	−0.11	−1.21	−0.22	8.10	9.66	7.53	8.52	−36.79	−3.53	−38.63	−6.96
	Europe	0.41	0.46	0.43	0.47	−0.62	0.53	−0.62	−0.15	5.11	6.31	5.07	5.28	−28.07	24.00	−28.09	−6.76
	Australia	0.61	0.61	0.61	0.64	−0.95	−0.46	−1.24	−0.51	7.40	7.80	7.15	7.37	−31.42	−15.31	−41.28	−16.89

forthcoming IMERG products for GPM users, as is being done in the current TRMM version 7.

SUMMARY AND OUTLOOK. A systematic evaluation of the recent four TMPA real-time datasets against the V7 research product from July 2008 to June 2011 shows that the latest version 7 TMPA-RT with climatological calibration has lower systematic biases and smaller random errors over both land and ocean relative to the other three versions of TMPA-RT estimates. From a global perspective, the version 7 TMPA calibration concepts could be considered as essentially ready for new measurements coming in the GPM era. However, both analyses indicate the current TRMM-era retrievals still have room for improvement. The CPC gauge-based analysis over four continental subregions showed higher RMSE values following application of the climatological calibration. While removing systematic bias at the monthly scales, the calibration scheme may have introduced deleterious effects on daily rainfall accumulations. This characteristic may have negative impacts for estimating heavy rainfall with high local variability at small scales. Another problem area was detected in high mountainous regions (e.g., the Himalayas) and high latitudes. The retrieval algorithms suffer from the effect of persistent snow cover and are generally less accurate in estimating falling snow. This highlights a word of caution when using the version 7 TMPA-RT estimates for monitoring precipitation over these specific zones and for highly variable extreme rainfall amounts. Although the newly introduced sensors and upgraded calibration algorithms have undoubtedly improved the TMPA's accuracy, some challenging issues in satellite retrieval processes will continue to remain open for the satellite QPE-hydrology community, providing the impetus for more research and development.

The GPM is a unique and complex program. The successful integration of the GPM Core Observatory instruments will substantially change the sensor composition and intercalibration scheme available for multisatellite estimation. Relative to TRMM, GPM is designed to make more accurate and frequent observations of global rainfall, especially over middle and high latitudes (Hou et al. 2014). Now, the GPM project is adopting the new Goddard profiling algorithm (a multichannel physical approach that has been named GPROF2014) to unify all of the available microwave observations over the latitude band 68°N/S so as to provide, for the first time, adequate sampling and accuracy of precipitation (both rain and snow) as calibrators beyond TRMM's 37°N/S band. During the satellite checkout, most activities are focused on the GPM-era algorithm development and validation with respect to the recent updates. One of the immediate tasks at hand is to complete the current testing and validation of the dual-frequency radar algorithm to derive characteristics of the raindrop spectra. Other important tasks for obtaining global precipitation estimates include extending quantitative precipitation estimation to higher latitudes and higher elevations and further improving the retrievals during winter months. With respect to the current monitoring skills, it is almost certain that regions characterized by complex terrain and snowy/ice cover will still be problematic for the day-1 multisatellite retrieval in GPM.

In summary, we expect that the global analysis of TRMM-based precipitation estimates reported here can give the satellite precipitation users a better understanding of the error features associated with currently available TMPA real-time precipitation estimates from a broader perspective. These results will better guide those users who are taking advantage of these satellite-based quantitative precipitation data to accommodate their various research and operational applications.

ACKNOWLEDGMENTS. This work was financially supported by National Science Foundation of China (51379056). The TMPA data used in this study were provided by the NASA Goddard Space Flight Center's Mesoscale Atmospheric Processes Laboratory and PPS, which develop and compute the TMPA as a contribution to TRMM. The authors thank three anonymous reviewers, who helped to improve the earlier version of this paper.

REFERENCES

Allen, M. R., and W. J. Ingram, 2002: Constraints on future changes in climate and the hydrologic cycle. *Nature,* **419,** 224–232, doi:10.1038/nature01092.

Behrangi, A., B. Khakbaz, T. C. Jaw, A. Aghakouchak, K. Hsu, and S. Sorooshian, 2011: Hydrologic evaluation of satellite precipitation products over a mid-size basin. *J. Hydrol.,* **397,** 225–237, doi:10.1016/j.jhydrol.2010.11.043.

Bitew, M. M., and M. Gebremichael, 2011: Evaluation of satellite rainfall products through hydrologic simulation in a fully distributed hydrologic model. *Water Resour. Res.,* **47,** W06526, doi:10.1029/2010WR009917.

Bunde, A., U. Büntgen, J. Ludescher, J. Luterbacher, and H. von Storch, 2013: Is there memory in precipitation? *Nat. Climate Change,* **3,** 174–175, doi:10.1038/nclimate1830.

Chen, M., W. Shi, P. Xie, V. B. S. Silva, V. E. Kousky, R. W. Higgins, and J. E. Janowiak, 2008: Assessing objective techniques for gauge-based analyses of global daily precipitation. *J. Geophys. Res.,* **113,** D04110, doi:10.1029/2007JD009132.

Chen, S., and Coauthors, 2013a: Similarity and difference of the two successive V6 and V7 TRMM Multisatellite Precipitation Analysis (TMPA) performance over China. *J. Geophys. Res. Atmos.,* **118,** 13 060–13 074, doi:10.1002/2013JD019964.

——, and Coauthors, 2013b: Evaluation of the successive V6 and V7 TRMM Multisatellite Precipitation Analysis over the continental United States. *Water Resour. Res.,* **49,** 8174–8186, doi:10.1002/2012WR012795.

Ebert, E. E., J. E. Janowiak, and C. Kidd, 2007: Comparison of near-real-time precipitation estimates from satellite observations and numerical models. *Bull. Amer. Meteor. Soc.,* **88,** 47–64, doi:10.1175/BAMS-88-1-47.

Gourley, J. J., Y. Hong, Z. L. Flamig, L. Li, and J. Wang, 2010: Intercomparison of rainfall estimates from radar, satellite, gauge, and combinations for a season of record rainfall. *J. Appl. Meteor. Climatol.,* **49,** 437–452, doi:10.1175/2009JAMC2302.1.

——, and Coauthors, 2013: A unified flash flood database over the United States. *Bull. Amer. Meteor. Soc.,* **94,** 799–805, doi:10.1175/BAMS-D-12-00198.1.

Habib, E., A. Henschke, and R. F. Adler, 2009: Evaluation of TMPA satellite-based research and real-time rainfall estimates during six tropical-related heavy rainfall events over Louisiana, USA. *Atmos. Res.,* **94,** 373–388, doi:10.1016/j.atmosres.2009.06.015.

——, M. ElSaadani, and A. T. Haile, 2012: Climatology-focused evaluation of CMORPH and TMPA satellite rainfall products over the Nile basin. *J. Appl. Meteor. Climatol.,* **51,** 2105–2121, doi:10.1175/JAMC-D-11-0252.1.

Hong, Y., R. F. Adler, and G. Huffman, 2007: An experimental global prediction system for rainfall-triggered landslides using satellite remote sensing and geospatial datasets. *IEEE Trans. Geosci. Remote Sens.,* **45,** 1671–1680, doi:10.1109/TGRS.2006.888436.

Hossain, F., and D. P. Lettenmaier, 2006: Flood prediction in the future: Recognizing hydrologic issues in anticipation of the Global Precipitation Measurement mission. *Water Resour. Res.,* **42,** W11301, doi:10.1029/2006WR005202.

Hou, A. Y., and Coauthors, 2014: The Global Precipitation Measurement (GPM) Mission. *Bull. Amer. Meteor. Soc.,* **95,** 701–722, doi:10.1175/BAMS-D-13-00164.1.

Huffman, G. J., and Coauthors, 2007: The TRMM Multisatellite Precipitation Analysis (TMPA): Quasi-global, multiyear, combined-sensor precipitation estimates at fine scales. *J. Hydrometeor.,* **8,** 38–55, doi:10.1175/JHM560.1.

——, R. F. Adler, D. T. Bolvin, and E. J. Nelkin, 2010: The TRMM Multi-satellite Precipitation Analysis (TMPA). Satellite Applications for Surface Hydrology. F. Hossain and M. Gebremichael, Eds., Springer, 3–22, doi:10.1007/978-90-481-2915-7_1.

Khan, S. I., and Coauthors, 2011: Satellite remote sensing and hydrologic modeling for flood inundation mapping in Lake Victoria Basin: Implications for hydrologic prediction in ungauged basins. *IEEE Trans. Geosci. Remote Sens.,* **49,** 85–95, doi:10.1109/TGRS.2010.2057513.

Kidd, C., and G. J. Huffman, 2011: Global precipitation measurement. *Meteor. Appl.,* **18,** 334–353, doi:10.1002/met.284.

——, V. Levizzani, J. Turk, and R. Ferraro, 2009: Satellite precipitation measurements for water resource monitoring. *J. Amer. Water Resour. Assoc.,* **45,** 567–579, doi:10.1111/j.1752-1688.2009.00326.x.

——, P. Bauer, J. Turk, G. J. Huffman, R. Joyce, K.-L. Hsu, and D. Braithwaite, 2012: Intercomparison of high-resolution of precipitation products over northwest Europe. *J. Hydrometeor.,* **13,** 67–83, doi:10.1175/JHM-D-11-042.1.

Lin, X., and A. Y. Hou, 2008: Evaluation of coincident passive microwave rainfall estimates using TRMM PR and ground measurements as references. *J. Appl. Meteor.,* **47,** 3170–3187, doi:10.1175/2008JAMC1893.1.

Liu, J., B. Wang, M. A. Cane, S. Y. Yim, and J. Y. Lee, 2013: Divergent global precipitation changes induced by nature versus anthropogenic forcing. *Nature,* **493,** 656–659, doi:10.1038/nature11784.

Min, S. K., X. Zhang, F. W. Zwiers, and G. C. Hegerl, 2011: Human contribution to more-intense precipitation extremes. *Nature,* **470,** 378–381, doi:10.1038/nature09763.

Romilly, T. G., and M. Gebremichael, 2011: Evaluation of satellite rainfall estimates over Ethiopian river basins. *Hydrol. Earth Syst. Sci.,* **15,** 1505–1514, doi:10.5194/hess-15-1505-2011.

Rudolf, B., H. Hauschild, W. Rueth, and U. Schneider, 1994: Terrestrial precipitation analysis: Operational method and required density of point measurements. *Global Precipitations and Climate Change,* M. Desbois and F. Désalmand, Eds., Springer, 173–186, doi:10.1007/978-3-642-79268-7_10.

Stisen, S., and I. Sandholt, 2010: Evaluation of remote-sensing-based rainfall products through predictive capability in hydrological runoff modelling. *Hydrol. Processes,* **24,** 879–891, doi:10.1002/hyp.7529.

Su, F., Y. Hong, and D. P. Lettenmaier, 2008: Evaluation of TRMM Multisatellite Precipitation Analysis

(TMPA) and its utility in hydrologic prediction in the La Plata basin. *J. Hydrometeor.,* **9,** 622–640, doi:10.1175/2007JHM944.1.

Tang, L., Y. Tian, and X. Lin, 2014: Validation of precipitation retrievals from satellite-based passive microwave sensors. *J. Geophys. Res. Atmos.,* **119,** 4546–4567, doi:10.1002/2013JD020933.

Tapiador, F. J., and Coauthors, 2012: Global precipitation measurement: Methods, datasets and applications. *Atmos. Res.,* **104–105,** 70–97, doi:10.1016/j.atmosres.2011.10.021.

Tian, Y., and C. D. Peters-Lidard, 2010: A global map of uncertainties in satellite-based precipitation measurements. *Geophys. Res. Lett.,* **37,** L24407, doi:10.1029/2010GL046008.

——, and Coauthors, 2009: Component analysis of errors in satellite-based precipitation estimates. *J. Geophys. Res.,* **114,** D24101, doi:10.1029/2009JD011949.

Tobin, K. J., and M. E. Bennett, 2010: Adjusting satellite precipitation data to facilitate hydrologic modeling. *J. Hydrometeor.,* **11,** 966–978, doi:10.1175/2010JHM1206.1.

Villarini, G., and W. F. Krajewski, 2007: Evaluation of the research version TMPA three-hourly 0.25° × 0.25° rainfall estimates over Oklahoma. *Geophys. Res. Lett.,* **34,** L05402, doi:10.1029/2006GL029147.

Wentz, F., L. Ricciardulli, K. Hilburn, and C. Mears, 2007: How much more rain will global warming bring? *Science,* **317,** 233–235, doi:10.1126/science.1140746.

Wu, H., R. F. Adler, Y. Hong, Y. Tian, and F. Policelli, 2012: Evaluation of global flood detection using satellite-based rainfall and a hydrologic model. *J. Hydrometeor.,* **13,** 1268–1284, doi:10.1175/JHM-D-11-087.1.

Wu, P., N. Christidis, and P. Stott, 2013: Anthropogenic impact on Earth's hydrological cycle. *Nat. Climate Change,* **3,** 807–810.

Xie, P., A. Yatagai, M. Chen, T. Hayasaka, Y. Fukushima, C. Liu, and S. Yang, 2007: A gauge-based analysis of daily precipitation over East Asia. *J. Hydrometeor.,* **8,** 607–626, doi:10.1175/JHM583.1.

——, M. Chen, and W. Shi, 2010: CPC unified gauge-based analysis of global daily precipitation. *24th Conf. on Hydrology,* Atlanta, GA, Amer. Meteor. Soc., 2.3A. [Available online at https://ams.confex.com/ams/90annual/techprogram/paper_163676.htm.]

Yong, B., L.-L. Ren, Y. Hong, J.-H. Wang, J. J. Gourley, S.-H. Jiang, X. Chen, and W. Wang, 2010: Hydrologic evaluation of Multisatellite Precipitation Analysis standard precipitation products in basins beyond its inclined latitude band: A case study in Laohahe basin, China. *Water Resour. Res.,* **46,** W07542, doi:10.1029/2009WR008965.

——, Y. Hong, L.-L. Ren, J. J. Gourley, G. J. Huffman, X. Chen, W. Wang, and S. I. Khan, 2012: Assessment of evolving TRMM-based multisatellite real-time precipitation estimation methods and their impacts on hydrologic precipitation in a high latitude basin. *J. Geophys. Res.,* **117,** D09108, doi:10.1029/2011JD017069.

——, and Coauthors, 2013: First evaluation of the climatological calibration algorithm in the real-time TMPA precipitation estimates over two basins at high and low latitudes. *Water Resour. Res.,* **49,** 2461–2472, doi:10.1002/wrcr.20246.